Electrospun pH-sensitive core-shell polymer nanocomposites fabricated using a tri-axial process

Chen Yang [a], Deng-Guang Yu [a,*], Deng Pan [a], Xin-Kuan Liu [a], Xia Wang [a], S.W. Annie Bligh [b], Gareth R. Williams [c,*]

[a] School of Materials Science & Engineering, University of Shanghai for Science and Technology, 516 Jungong Road, Shanghai 200093, China.
[b] Faculty of Science and Technology, University of Westminster, 115 New Cavendish Street, London W1W 6UW, UK.
[c] UCL School of Pharmacy, University College London, 29-39 Brunswick Square, London WC1N 1AX, UK.

* **Corresponding authors:**
Prof. Deng-Guang Yu and Dr. Gareth R. Williams

Addresses:
DGY:
School of Materials Science & Engineering,
University of Shanghai for Science and Technology,
516 Jungong Road, Yangpu District,
Shanghai 200093, P.R. China
Tel: +86-21-55270632
Fax: +86-21-55270632
Email: ydg017@usst.edu.cn

GRW:
UCL School of Pharmacy
University College London
29-39 Brunswick Square
London
WC1N 1AX
Tel: +44 207 753 5868
Email: g.williams@ucl.ac.uk

Abstract:

A modified tri-axial electrospinning process was developed for the generation of a new type of pH-sensitive polymer/lipid nanocomposite. The systems produced are able to promote both dissolution and permeation of a model poorly water-soluble drug. First, we show that it is possible to run a tri-axial procress with only one of the three fluids being electrospinnable. Using an electrospinnable middle fluid of Eudragit S100 (ES100) with pure ethanol as the outer solvent and an unspinnable lecithin-diclofenac sodium (PL-DS) core solution, nanofibers with linear morphology and clear core/shell structures can be fabricated continuously and smoothly. X-ray diffraction proved that these nanofibers are structural nanocomposites with the drug present in an amorphous state. *In vitro* dissolution tests demonstrated that the formulations could preclude release in acidic conditions, and that the drug was released from the fibers in two successive steps at neutral pH. The first step is the dissolution of the shell ES100 and the conversion of the core PL-DS into sub-micron sized particles. This frees some DS into solution, and later the remaining DS is gradually released from the PL-DS particles through diffusion. *Ex vivo* permeation results showed that the composite nanofibers give a more than two-fold uplift in the amount of DS passing through the colonic membrane as compared to pure DS; 74% of the transmitted drug was in the form of PL-DS particles. The new tri-axial electrospinning process developed in this work provides a platform to fabricate structural nanomaterials, and the core-shell polymer-PL nanocomposites we have produced have significant potential applications for oral colon-targeted drug delivery.

Keywords: Tri-axial electrospinning; core-sheath fibers; polymer-lipid nanocomposites; colon-targeted drug delivery; electrospinnability

1. Introduction

The fabrication of advanced drug delivery systems (DDSs) is increasingly dependent on the creation of complex architectures and understanding structure-activity relationships at the nanoscale [1-3]. To this end, core-shell nanostructures have been very widely studied in the production of functional nanomaterials, including those for biomedical applications [4-6]. For drug delivery and controlled release, both the core and shell can be loaded with an active pharmaceutical ingredient (API) and/or with different types of pharmaceutical excipients. Applications of such systems include improving the solubility of poorly water-soluble drugs, controlled release of multiple APIs from a single dosage form, or tunable multiple phase release [7-9].

Over recent years, polymers and lipids have been the most widely used pharmaceutical excipients, and these materials have acted as the basis for a broad gamut of novel DDSs, being exploited to alter the biopharmaceutical and pharmacokinetic properties of the drug molecule for favorable clinical outcomes [3,10,11]. Numerous core-shell polymeric nanoparticles (NPs) and lipid-based DDS (such as solid lipid dispersions and liposomes) have been investigated for drug delivery through varied administration routes [12-15]. Novel strategies derived from the combined usage of polymers and phospholipids (PLs) have been reported for some biomedical applications (including controlled release) and are presently of intense interest in the pharmaceutics field. However, virtually all the reported polymer-lipid composites are in the form of microparticles or NPs [4,8,16-18].

Core-shell nanofiber-based DDS have received relatively little attention, and to the best of our knowledge there are no reports of drug-loaded polymer-lipid nanofibers being used in drug delivery.

Electrospun nanofibers, comprising an API loaded into a filament-forming polymer, have been the focus of much research. They are prepared from a co-dissolving solution of a drug and polymer; this is ejected from a syringe with electrical energy used to rapidly evaporate the solvent and yield one-dimensional fibers with diameters frequently on the nanoscale. This technique is scalable, and several recent reports address large scale fabrication and the potential for commercial products [19-22]. The intense research effort invested in these materials thus appears to be about to yield products which can make a major difference to patients' lives. Electrospinning is a facile, one-step procedure, and the products form as a visible and flexible mat which can easily be recovered from the collector without significant loss of material or damage. The nanofibers produced can further be used as templates to manipulate molecular self-assembly to create drug-loaded NPs or liposomes; the electrospinning technique thus provides not only a bridge between fiber-based and NP-based DDSs, but also between solid and liquid dosage forms [23-26].

The most simple, single-fluid, electrospinning process has been explored for approaching two decades, and the applications of the resultant monolithic nanofibers have been probed in a wide range of fields. Current developments in electrospinning are focused in two key areas. The first is the manufacture of electrospun nanofibers on an industrial scale [27-29]. The second line of research involves developing advanced electrospinning techniques to yield nanofibers with sophisticated structural characteristics (such as multiple-compartment nanofibers, core-shell nanofibers, or structured fibers with varied distributions of the API), which in turn impart tunable and multiple functionalities [30-32]. Because of the popularity of core-shell nanostructures and the relative ease of the process, coaxial electrospinning (in which two needles, one nested inside another, are used to handle two working fluids) has been the focus of much research. Other advanced approaches such as side-by-side electrospinning (to yield Janus fibers), tri-axial electrospinning (giving three-layer composites), and other types of multiple-fluid electrospinning have been neglected in comparison [6,9,33].

Compared with single-fluid electrospinning, the standard coaxial experiment has greatly expanded the range of fibers which can be produced. These include not only core-shell fibers [34,35], but also fibers prepared from materials without filament-forming properties [36] and used as templates for creating nanotubes (from the fiber as a whole) or the “bottom-up” generation of NPs (self-assembled from the components loaded in the fibers) [26, 37]. For biomedical applications, core-shell nanofibers proffer a series of new possibilities; for instance, it is possible to protect a fragile active ingredient such as a protein from the stresses of the electrospinning processes by confining it to the core, or to vary the APIs concentration in the core and shell to achieve complex drug release profiles [38-41]. In the traditional coaxial process the sheath working fluid must be electrospinnable, but a modified process in which one can utilize unspinnable liquids as the sheath fluid is also possible. The number of polymers which can be directly electrospun is rather limited, but there are numerous unspinnable liquids, and the modified coaxial process should hence further expand the range of functional nanofibers which can be produced [38,42,43].

The above discussion is focused on the simultaneous processing of two fluids; working with three or even four fluids simultaneously is also possible, however [44-49]. For example, Han and Steckl reported tri-layer nanofibers for biphasic controlled release, using dyes as model active ingredients [49]. In very recent work, we successfully developed a tri-axial electrospinning process to generate nanofibers with a gradient distribution of the API, allowing us to achieve zero-order drug release profiles [31]. However, in all the tri-axial electrospinning processes reported to date, the three working fluids are all electrospinnable. This limits the applications of the process. If unspinnable liquids can be processed in combination with spinnable working solutions, a much broader selection of functional products could be designed and generated.

Building on our previous work developing modified coaxial [38,42,43] and standard tri-axial electrospinning [50], here we report the first modified tri-axial electrospinning process. We have used this process to create core-shell fibers comprising a lipid-drug core and a pH sensitive shell, thereby allowing us to demonstrate that only an electrospinnable central fluid is required to achieve a successful tri-axial process. The polymer-lipid nanocomposites produced showed desirable functional performance in altering the release behavior of the model drug diclofenac sodium and improving its permeation through the colonic membrane.

2 Experimental

2.1. Materials

Eudragit S100 (ES100, M_w=135,000), a methacrylic acid/methyl methacrylate copolymer which only dissolves at pH > 7.0, was obtained from Röhm GmbH (Darmstadt, Germany). Diclofenac sodium (DS, a non-steroidal anti-inflammatory drug with potent anti-inflammatory, analgesic and antipyretic properties) was purchased from the Hubei Biocause Pharmaceutical Co., Ltd. (Hubei, China). Lecithin (PL, extracted from egg yolk, and containing lysophosphatidylcholine, sphingomyelin, and neutral lipids in minor quantities), N,N-dimethylacetamide (DMAc), anhydrous ethanol, methylene blue and basic fuchsin were purchased from the Sinopharm Chemical Reagent Co., Ltd. (Shanghai, China). All other chemicals used were analytical grade, and water was doubly distilled before use.

2.2. Electrospinning

The tri-layer concentric spinneret was homemade. Three syringe pumps (KDS100, Cole-Parmer, Vernon Hills, IL, USA) and a high-voltage power supply (ZGF 60kV/2 mA, Shanghai Sute Corp., Shanghai, China) were used for electrospinning. The collector comprised a flat piece of cardboard wrapped with aluminum foil. All electrospinning processes were carried out under ambient conditions (21 ± 5 °C with a relative humidity of 47 ± 5 %). Experiments were recorded using a digital camera (PowerShot A490, Canon, Tokyo, Japan). The spinneret to collector distance was fixed at 15 cm for all experiments.

The outer fluid was pure anhydrous ethanol. The middle fluid consisted of 14.0 g

ES100 in 100 mL of a mixture of ethanol / DMAc (90:10 v/v). The inner fluid was prepared from 3 g PL and 0.6 g DS in 10 mL ethanol. After initial optimization experiments, the applied voltage was fixed at 15 kV. To facilitate observation of the electrospinning processes, 10 mg/L methylene blue was added to the inner fluid and 5 mg/L basic fuchsin to the middle fluid. Four different sets of fibers were prepared with varied flow rates, as detailed in Table 1.

Table 1. Key details of the electrospinning processes and resultant fibers

No.	Process	F_O[a] (mL/h)	F_M[a] (mL/h)	F_I[a] (mL/h)	Morphology[b]	Diameter (μm)
F1	Single	0	3.0	0	Linear	1.27± 0.13
F2	Tri-axial	0.5	2.0	0.5	LInear	0.55±0.06
F3		0.5	1.6	0.9	Linear, with some beads	0.47±0.05
F4		1.0	1.6	0.4	Spindles-on-a-string	----

2.3. Characterization

2.3.1. Morphology

The morphology of the fibers was determined using a Quanta FEG450 field emission scanning electron microscope (FESEM; FEI Corporation, Hillsboro, OR, USA). Prior to examination, samples were gold sputter-coated under a nitrogen atmosphere to render them electrically conductive. Images were recorded at an excitation voltage of 20 kV. The average fiber size was determined by measuring their diameters at more than 100 places in FESEM images, using the NIH Image J software (National Institutes of Health, MD, USA). To view the cross-sections of sample F2, a section of the fiber mat was placed into liquid nitrogen and manually broken before gold coating.

Transmission electron microscope (TEM) images of the samples were recorded on a JEM 2100F field emission TEM (JEOL, Tokyo, Japan). Samples were collected by fixing a lacey carbon-coated copper grid on the collector and electrospinning directly onto it for several minutes.

2.3.2. Physical form and compatibility

X-ray diffraction (XRD) was conducted using a D/Max-BR diffractometer (Rigaku, Tokyo, Japan) with Cu Kα radiation over the 2θ range 5 to 60° at 40 kV and 30 mA. Attenuated total reflectance-Fourier transform infrared (ATR-FTIR) spectroscopy was carried out on a Nicolet-Nexus 670 FTIR spectrometer (Nicolet Instrument Corporation, Madison, USA) from 500 cm^{-1} to 4000 cm^{-1} at a resolution of 2 cm^{-1}.

2.3.3. In vitro dissolution tests

To determine drug loading efficiency (LE), 0.100 g of the fibers was added into 10 mL of a 10% v/v ethanol solution in water, in order to extract all the loaded DS. The resultant solutions were diluted using phosphate buffered saline (PBS, pH7.0, 0.1M) to a suitable concentration for UV measurement. The LE was calculated using the following equation:

$$LE(\%) = (\text{DS mass measured})/(\text{theoretical DS mass in the formulation})\times 100\%$$

In vitro dissolution tests were carried out according to the Chinese Pharmacopoeia (2015 Ed.). Method II, which is a paddle method, was undertaken using a RCZ-8A dissolution apparatus (Tianjin University Radio Factory, Tianjin, China). 280 mg of fibers F2 or 20 mg of the DS raw material (particle size <30 μm) were first placed in 600 mL of 0.1 M HCl. Two hours later, 2.4 g NaOH was added to neutralize the dissolution media. The temperature of the dissolution medium was 37 ± 1 °C and the instrument was stirred at 50 rpm. Sink conditions were maintained, with $C < 0.2C_s$. At predetermined time points, 5.0 mL aliquots were withdrawn from the dissolution medium and replaced with distilled water to maintain a constant volume. After filtration through a 0.22 μm membrane (Millipore, Billerica, MA, USA) and appropriate dilution with PBS, samples were analyzed at λ_{max} = 276 nm using a UV–vis spectrophotometer (UV-2102PL, Unico Instrument Co. Ltd., Shanghai, China). The cumulative amount of DS released at each time point was back-calculated from the data obtained against a predetermined calibration curve. Experiments were performed seven times, and the average results from six of these replicates are reported as mean ± S.D.

During the *in vitro* dissolution process, dissolution media from the seventh replicate was withdrawn and the transmittance at λ=500 nm measured using the UV–vis spectrophotometer. The average hydrodynamic diameter and size distribution of the particles in the final dissolution medium from these experiments were determined using a BI-200SM static and dynamic light scattering (SDLC) instrument (Brookhaven Instruments Corporation, Austin, TX, USA).

2.3.4. Ex vivo permeation tests

Ex vivo permeation studies were performed using a RYJ-6A diffusion test apparatus (Shanghai Huanghai Drug Control Instrument Co., Ltd., Shanghai, China), in which materials were mounted in six Keshary-Chien glass diffusion cells and a water bath system maintained a constant temperature of 37 ± 0.2 °C. Each cell had a diffusion area of 2.60 cm^2, and the receptor compartment had a capacity of 7.2 mL PBS (pH7.0, 0.1M). Each donor compartment was filled with 1.0 mL PBS and the hydrodynamics in the receptor compartment were maintained by stirring at 50 rpm with a Teflon coated magnetic bead. Large intestines were obtained from pigs after slaughtering (Baoshan Jiangwan slaughterhouse, Shanghai, China). The intestine was washed carefully with physiological saline solution (NaCl 0.9% w/v) to remove non-digested food. The colonic membranes were peeled away from the intestines and fixed on diffusion cells with the mucosal walls upward. They were equilibrated at 35 °C for 30 min before permeation tests.

The F2 fibers (140 mg) were placed on the mucosal surface in the chambers. Samples (1 mL) were withdrawn from the receptor compartment at timed intervals and 1 mL fresh PBS was added to maintain the volume of fluid here at a constant level. The aliquots were filtered through a 0.22 μm membrane (Millipore, Billerica, MA, USA). The absorption of the filtrate was measured at 276 nm to determine the amount of DS present in the aqueous phase. The semi-solid residue was dissolved using 10 mL of a 10% v/v ethanol solution in water and diluted with PBS before measuring absorbance, in order to determine its DS content of. All measurements were carried out in triplicate. Permeation experiments with 10 mg of pure DS (particle size <30 μm) as a control were also carried out.

2.4. Statistical analysis

The experimental data are presented as mean ± SD. The results from the *in vitro* dissolution tests and *ex vivo* permeation tests were analyzed using one-way ANOVA. The threshold significance level was set at 0.05. Thus, *p* (probability) values lower than 0.05 were considered statistically significant.

3. Results and discussion

3.1. Implementation of modified tri-axial electrospinning

A diagram illustrating the modified tri-axial electrospinning process is shown in Fig. 1. The system consists of four components: three syringe pumps to drive the working fluids, a power supply, a fiber collector, and a three layer concentric spinneret. In modified coaxial electrospinning, the use of a spinnable core solution can ensure a successful process regardless of the electrospinnability of the sheath fluid [43]. Here, the central solution is electrospinnable, and this is utilized to achieve tri-axial electrospinning even though the outer fluid is pure solvent and the inner fluid is unspinnable.

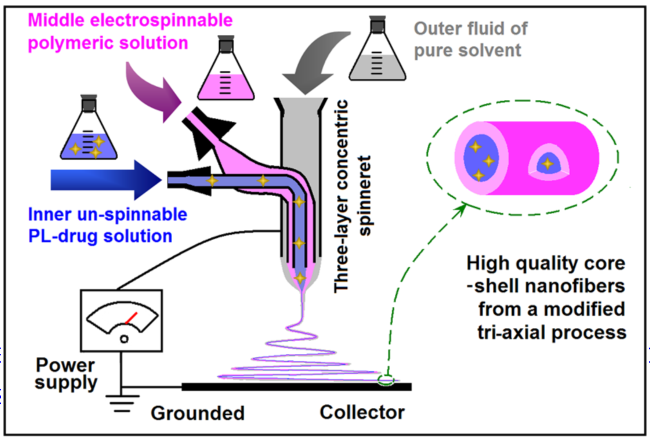

Fig. 1 A diagra… …ess and its use for preparing core-s…

The homemade tri-concentric spinneret and its connection with the power supply and three working fluids are shown in Fig. 2a. An alligator clip was used to connect the power supply to the spinneret, which was directly fixed to the syringe holding the outer fluid. The middle and inner fluids were connected to the spinneret through high-elastic silicon tubing.

The design of the spinneret is of critical importance in ensuring a robust and reproducible electrospinning process [42,48]. A well-designed spinneret must provide a suitable template for producing the desired nanofiber architectures, and must be developed bearing in mind the behavior of the working fluids under an electrical field. The spinneret used in this work is exhibited in the top-right and bottom-right insets of Fig. 2a. It consists of three concentric capillaries composed of austentic stainless steel ($O_6Cr_{19}Ni_{10}$, GB24511 in China). The inner, middle and outer capillaries have outer diameters of 0.4, 1.6, 2.8 mm and inner diameters (D_i) of 0.20, 1.3 and 2.2 mm, respectively. The end of the inner capillary projects 0.2 mm out of the central one, which similarly projects 0.2 mm from the outer capillary. This design helps to ensure the encapsulation of the inner fluid by the middle fluid, and in turn the middle by the outer fluid. This structure should also help to prevent mixing of the working fluids when they are ejected from the spinneret.

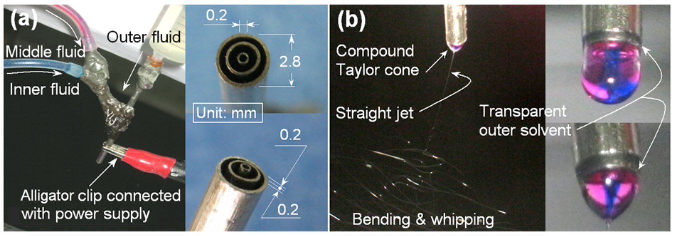

Fig, 2. The implementation of modified tri-axial electrospinning: (a) the connection of the spinneret with the power supply and the working fluids (left), and images of the tri-concentric spinneret (insets); (b) a digital photograph of the tri-axial process (left), the tri-layer droplet before a voltage of 15 kV was applied (top-right) and the compound Taylor cone (bottom-right).

Under optimised conditions (see Section 2.2), successful electrospinning could be achieved as shown in Fig. 2b. The process involves three steps including Taylor cone formation, the emission of a straight fluid jet and then an unstable region with gradually enlarged bending and whipping loops. The top-right inset of Fig. 2b displays the droplets ejected from the spinneret with no voltage applied. Both the blue inner fluid and pink middle fluids were observed to diffuse into the outer fluid to some extent, as demonstrated by their gradually increased sizes and decreased size of the outer (colourless) solvent moving away from the spinneret. However, the three working fluids form a clear three-layer compound Taylor cone when a voltage of 15 kV was applied, as shown in the bottom-right inset of Fig. 2b.

The modified tri-axial electrospinning process can be run continuously and smoothly, without any clogging or other adverse phenomena arising. These are frequently encountered in traditional single-fluid and coaxial electrospinning [50], but spinning with a pure solvent as the exterior fluid has been shown to reduce incidents of clogging as well as to improve the uniformity of the fibers produced in the latter process [42]. The use of pure solvent as the outer layer will: 1) lubricate the spinneret to retard clinging; 2) prevent the formation of semi-solid substance on the surface of the fluid jets; 3) protect the inner fluid from any environmental fluctuations; and, 4) lead to a longer drawing period under the electrical field, and thus to narrower fibers.

3.2. Morphology and core-shell structures of the created nanofibers

FESEM images of fibers F1 to F4 are shown in Fig. 3. When the inner and outer fluids were turned off, a traditional single-fluid electrospinning of the middle ES100 solution could be achieved. Although manual intervention was needed periodically to remove semi-solid substances which collected on the spinneret, the resultant ES100 fibers were linear without any beads-on-a-string or spindles-on-a-string morphology (Fig. 3a1 and 3a2). These fibers have an average diameter of 1.27 ± 0.13 μm, with an uneven and wrinkled surface (Table 1, Fig. 3a2). This is a result of barometric pressure, when residual solvent which was not evaporated during electrospinning escaped from the fibers. Single-fluid electrospinning easily traps solvent in the fibers because of the formation of a solid "skin" on the fluid jet during the solidification process.

The F2 fibers are linear with an average diameter of 0.55 ± 0.06 μm and smooth surfaces (Fig. 3b1 and 3b2, Table 1). This can be attributed to the surrounding outer solvent and appropriate selection of the flow rates of the three working fluids (0.5, 2.0 and 0.5 mL/h for outer, middle and inner fluids, respectively). If the flow rate of the outer solvent is kept constant and those of the middle and inner fluid altered to 1.6 and 0.9 mL/h respectively, the resultant F3 material has many beads clinging to the fibers, although the latter are still linear with an average size of 0.47 ± 0.05 μm (Fig. 3b1 and 3b2, Table 1). It is thought that this high flow rate of the inner fluid causes it to penetrate the middle and outer fluids to form round PL-DS beads on the fiber surfaces.

If the flow rate of the outer solvent is doubled to 1.0 mL/h, the fibers generated exhibit a typical spindles-on-a-string morphology (Fig. 3d1 and 3d2). Some unexpected clumps are also formed within the fiber mat, as shown in the inset of Fig. 3d1. These are ascribed to PL escaping from the inner fluids. A further increase of the outer solvent flow rate was found to result in an electrospraying process. These results demonstrate that the selection of flow rates is a key parameter which must be controlled to ensure the formation of a core-shell nanostructure.

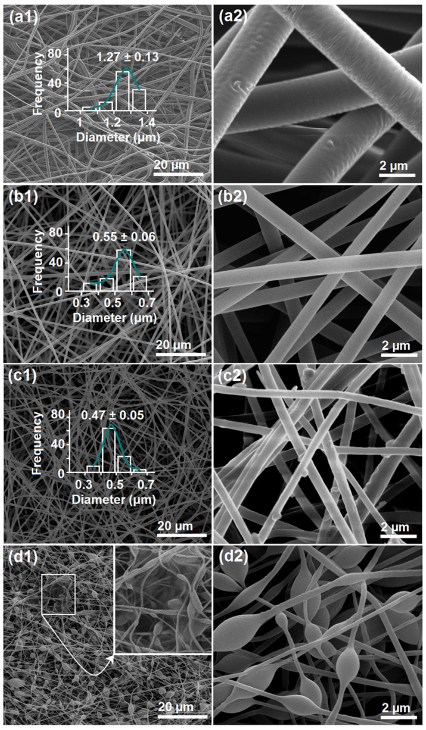

Fig. 3. FESEM images of the core-shell nanofibers and their size distributions; (a1 and a2) F1; (b1 and b2) F2; (c1 and c2) F3; (d1 and d2) F4, the inset shows a clump of PL-DS.

FESEM images of cross-sections of F2 (Fig. 4a) and TEM images (Fig. 4b) demonstrate that the fibers have clear core/shell structures. Both the FESEM and TEM images suggest that the PL-DS core has a diameter of approximately 300 nm.

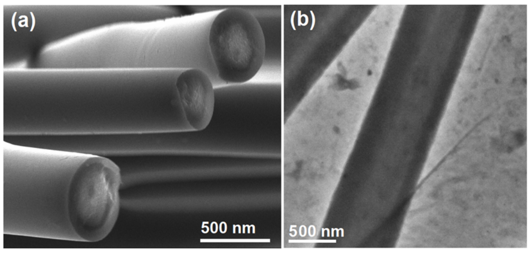

Fig. 4. (a) A FESEM and (b) TEM image of the cross-sections of F2.

3.3. Physical form and component compatibility

XRD data are depicted in Fig. 5; these clearly demonstrate that DS is crystalline, with many sharp Bragg reflections visible in its pattern. ES100 exhibits only a broad hump, characteristic of an amorphous material. PL exists as a paste at an ambient temperature of 21 °C, yet shows a sharp reflection at $2\theta=5.18^{\circ}$. This suggests that there are liquid crystals present in the PL paste, with an ordered lamellar structure as reported in the early literature [51]. All reflections from PL and DS are absent in the patterns of the core-shell F2 fibers, suggesting the formation of an amorphous PL-DS complex.

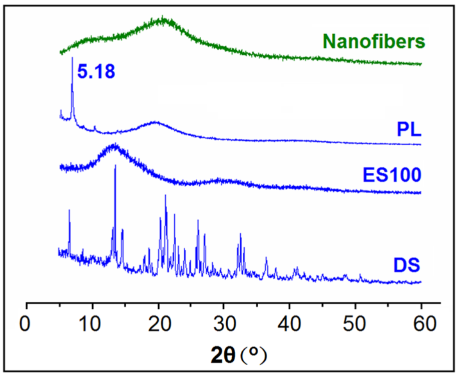

Fig. 5. XRD patterns of the raw materials (PL, EL100 and DS) and F2.

The potential secondary interactions between the fiber components were investigated using ATR-FTIR, and the results are shown in Fig. 6. DS has three characteristic peaks at 1574, 1553 and 1507 cm^{-1} arising from its benzene rings. In the spectrum of PL, the CH_2 symmetric and asymmetric vibrations at 2854 cm^{-1} and 2923 cm^{-1} and the antisymmetric stretch of $N^+(CH_3)_3$ at 968 cm^{-1} comprise the most prominent features. These peaks similarly appear in the spectrum of the fibers, confirming the presence of PL with ES100. However, the characteristic peaks from the benzene rings of DS cannot be seen in the F2 spectrum. This can be attributed to secondary interactions between PL and DS. Hydrophobic interactions, in addition to possible hydrogen bonding and electrostatic interactions, can arise between all three components in F2, as is clear from a consideration of the molecular structures in Fig. 6. These secondary interactions should ensure that the drug and excipients are highly compatible, favorable for the stability of the core-shell nanocomposites.

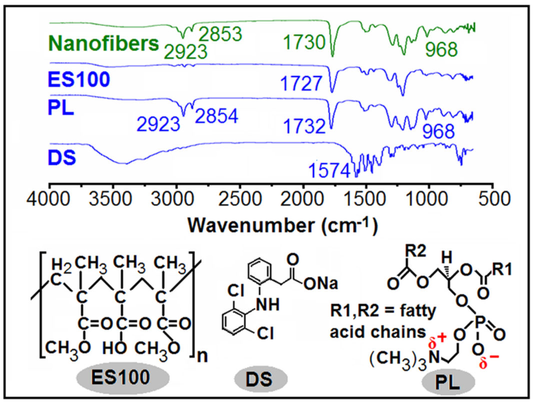

Fig. 6. ATR-FTIR spectra and the molecular formulae of the fiber components.

3.4. Functional performance

DS has a maximum absorbance at 276 nm, which was used to construct a calibration curve: A=0.0085+0.0279 C (R=0.9997) within a linear range from 2 to 50 μg/mL. The drug content in F2 was first assayed, and found to be 7.26 ± 0.31% (n = 6), almost identical to the calculated value of 7.14%.

The *in vitro* release profiles of F2 and the DS starting material are shown in Fig. 7a. DS is virtually insoluble in acidic conditions, with a small increase in solubility when the pH is raised to neutral. After 2 h in acid, 2.8% of DS from the raw material was freed into the dissolution media. When the pH was raised to neutral, the DS particles gradually dissolved over *ca.* 3 hours. For F2, 2.1% of the loaded DS was released during the first 2 h. In the neutral dissolution media, the nanofibers released a total of 79.1% of the incorporated DS over 22 h.

ES100 is a pH-sensitive polymer, and is insoluble at pHs below 7.0; it can thus be used to target DS to the colon region. DS is a popular API for oral administration and is frequently used in the treatment of pain and peri-operatively. However, it can easily result in an anaphylactic reaction, and to an allergic reaction in the digestive tract [52,53]. With traditional electrospun nanofibers, the drug is released by diffusion through an insoluble polymeric matrix, or by an erosion mechanism from a water-soluble carrier (or a combination of both processes) [39,43]. Here the drug release from the core-shell composites is expected to include two successive steps (Fig. 7b). First, dissolution of the pH-sensitive ES100 shell will occur, with some diffusion of DS from the insoluble core PL. After dissolution of the shell ES100, the core PL-DS is not thought to be able to endure the shear forces of stirring applied during the experiment and thus we propose that the core is broken up into PL-DS particles. The DS is then gradually released from the resultant DS-PL aggregates. Thus in the dissolution tests, the released drug (%) corresponds to the DS molecules which are in solution (the DS-PL aggregates in suspension are removed by filtration).

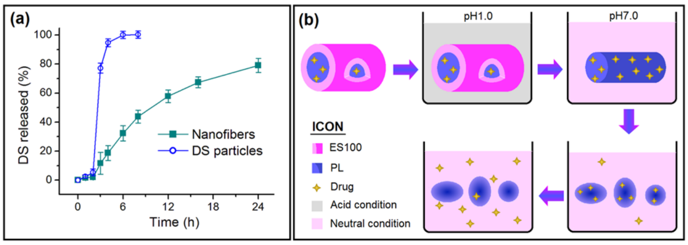

Fig. 7. *In vitro* dissolution of DS and D2 (a) and the proposed drug release mechanism (b).

To further investigate the drug release mechanism and validate this hypothesis, the transmittance of the dissolution media and light scattering studies were performed. The changes in transmittance at λ=500 nm are shown in Fig. 8a. DS has no absorbance above 320 nm, and thus any turbidity of the dissolution media recorded at this wavelength must result from the formation of a PL-DS suspension. In the first 2 h, the transmittance remains virtually constant. After the pH is raised to neutral, the transmittance values decreased for 3 h, after which they level out at around 77%. This is consistent with the dissolution of the shell ES100 occurring over this period and resulting in PL-DS nanoparticles.

The SDLC results obtained on the final dissolution medium are given in Fig. 8b. The PL-DS particles formed have an average diameter of 434 nm with a polydispersity index (PDI) of 0.187.

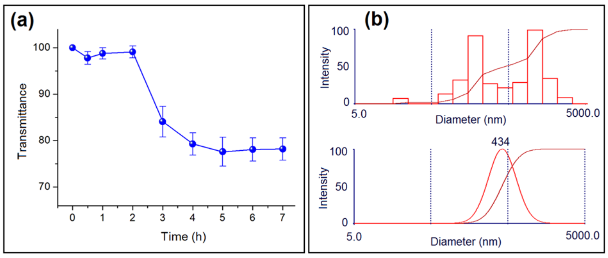

Fig. 8. (a) The transmittance of the dissolution medium measured at 500 nm as a function of time and (b) the sizes of the PL-DS particles measured by SDLC at the end of the dissolution experiment.

The results of permeation tests are presented in Fig. 9. DS is a Biopharmaceutical class II drug, meaning it is poorly water-soluble but is able to effectively cross fatty membranes [54]. After 12 h only 3.7 mg of the pure drug was transmitted into the receptor cells. The dissolution of DS is very slow because there is only a very limited amount of aqueous medium in the donor cell (*cf.* the dissolution experiments, which are performed under sink conditions) [55]. For the F2 fibers, both dissolved DS and the PL-DS particles penetrate the bio-membranes into the receptor cells [56]. Although the core-shell nanofibers provided sustained release of DS in dissolution studies (much slower than the release from pure DS), after 12 h 8.1 ± 0.46 mg DS from F2 had entered the receptor chamber. Of this amount, 1.7 ± 0.23 mg was present in the aqueous phase (or in particles below 220 nm in size, which could pass through the filters used). This suggests that (8.1-1.7)/8.1×100=79% of the DS penetrated through the mucosal membrane in the format of PL-DS particles. For oral administration applications, this drug delivery route should alleviate any potential allergic reactions with the digestive tracts.

Many commercial tablets are essentially a physical mixture of drug powders and polymeric carrier, the latter being added to modulate the drug release behavior. The combined use of polymer and lipid in the fibers prepared in the work is able to both protect the API from release in the stomach and provide sustained release in the colonic region, and also ensure improved trans-membrane permeability, leading to more effective absorbance. This strategy is particularly useful for oral delivery of Class IV drugs (which are both poorly water-soluble and have poor permeation properties). Drug-loaded electrospun fibers can easily be converted into routine oral solid dosage forms such as tablets and capsules using traditional pharmaceutical protocols [57-59].

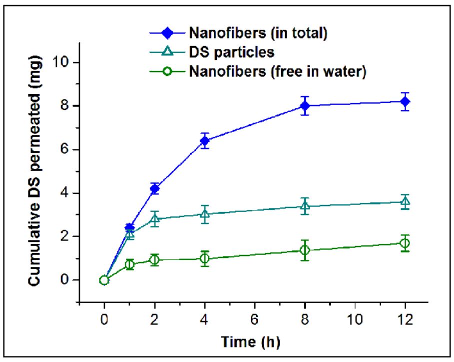

Fig. 9. *Ex vivo* permeation profiles of the F2 fibers and pure DS (n=6).

3.5. Perspectives

Coaxial electrospinning is often regarded as a major breakthrough in this field [60,61]. The fact that only one of the working fluids needs to be electrospinnable for a successful coaxial process significantly widens the range of materials which can be processed, and a very broad family of core-shell nanostructures can be produced. There are only about 100 polymers which can be directly electrospun into fibers, and often these can only be processed within a narrow window of conditions (concentration, voltage, etc). The introduction of unspinnable fluids in the modified coaxial processes greatly expands the capability of this simple technology to produce nanoscale products from a large range of raw materials. Furthermore, modified coaxial electrospinning permits all types of liquid phase (including solvents, small molecule solutions, dilute polymer solutions, suspensions and also emulsions) to be processed.

In this work, we report the first example of modified tri-axial electrospinning. Similar to modified co-axial spinning, this moves technology beyond the traditional tri-axial process in which all three working fluids are required to be individually electrospinnable. In our work, two of the three fluids were unspinnable alone: an electrospinnable middle layer fluid is sufficient to ensure a successful tri-axial process. This proof-of-concept work indicates that there are many possibilities in developing functional nanofibers through the introduction of unspinnable outer-layer and inner-layer working fluids into tri-axial processes.

The feasibility of the different tri-axial electrospinning processes which can be conceived are summarized in Fig. 10. A process with three spinnable working fluids (Process I) has been reported in several publications [31,44,45]. Processes II, III and IV have two of the three fluids being electrospinnable, and these are feasible provided the working fluids are compatible. This report is an example of Process V, with a spinnable middle layer fluid used to support unspinnable outer and inner fluids. For processes VI and VII, the two unspinnable fluids are adjacent to each other. This may result in diffusion of the solutes and formation of a mixture of the two unspinnable liquids, and thus it is anticipated that such to tri-axial electrospinning processes will result in failure.

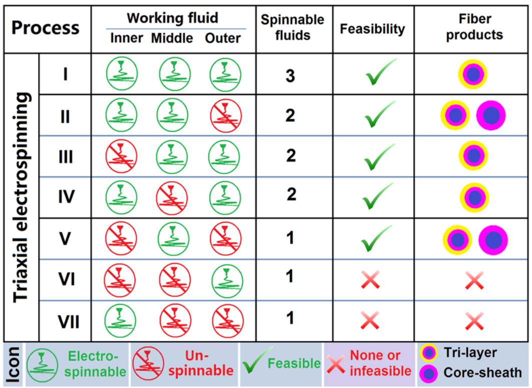

Fig. 10. The feasibility of different tri-axial electrospinning processes.

4. Conclusions

A modified tri-axial electrospinning process was successfully implemented to create core-shell nanofibers, in which a spinnable Eudragit S100 (ES100) solution was used as the middle fluid to support the outer solvent and an unspinnable phosphatidyl choline (PL)/diclofenac sodium (DS) inner solution. This resulted in a continuous and trouble-free nanofabrication process. The resultant core-shell nanofibers have a linear morphology with an obvious core-shell structure. XRD demonstrated that the nanofibers are structural nanocomposites with both the drug DS and also the lipid carrier PL losing their original crystalline physical forms and being transferred into an amorphous state. These core (PL-DS)-shell (ES100) nanostructures can protect the drug from release in acidic conditions to give colon-targeted release. They release the drug through two successive steps at neutral pH: first, dissolution of the shell ES100 occurs, which is believed to generate PL-DS sub-micron sized particles. Subsequently, release of DS from the particles occurs. The composite nanofibers lead to more than twice as much drug permeation through the colonic bio-membrane when compared with pure DS. The tri-axial electrospinning process developed in this work should provide a new platform to fabricate structural nanomaterials, and polymer-PL nanocomposites such as those prepared here can be utilized for effective oral drug delivery.

Acknowledgements

This work was supported by the China NSFC/UK Royal Society cost share international exchanges scheme (No. 51411130128/IE131748), the National Science Foundation of China (Nos. 51373101 and 51373100), the Natural Science Foundation of Shanghai (No. 13ZR1428900) and the Hujiang Foundation of China (No. B14006). DP and LXK are also indebted to the Key Laboratory of Advanced Metal-based Electrical Power Materials, Shanghai Municipal Commission of Education.

References

[1] Farokhzad OC, Langer R. Impact of nanotechnology on drug delivery. ACS Nano 2009;3:16-20.

[2] Lu Y, Chen SC. Micro and nano-fabrication of biodegradable polymers for drug delivery. Adv Drug Del Rev 2004;56:1621-1633.

[3] Mitragotri S, Burke PA, Langer R. Overcoming the challenges in administering biopharmaceuticals: formulation and delivery strategies. Nat Rev Drug Discov 2014;13:655-672.

[4] Sun J, Zhang L, Wang J, Feng Q, Liu D, Yin Q, Xu D, Wei Y, Ding B, Shi X, Jiang X. Tunable rigidity of (polymeric core)–(lipid shell) nanoparticles for regulated cellular uptake. Adv Mater 2015; 27:1402-1407.

[5] Liang X, Li J, Joo JB, Gutiérrez A, Tillekaratne A, Lee I, Yin Y, Zaera F. Diffusion through the shells of yolk–shell and core–shell nanostructures in the liquid phase. Angrew Chem Int Ed 2012;51:8034-8036.

[6] Chen G, Xu Y, Yu DG, Zhang DF, Chatterton NP, White KN. Structure-tunable Janus fibers fabricated using spinnerets with varying port angles. *Chem Commun* 2015;51:4623-3626.

[7] Bikiaris DN. Solid dispersions, Part II: new strategies in manufacturing methods for dissolution rate enhancement of poorly water-soluble drugs. Exp Opin Drug Del 2011; 8:1663-1680.

[8] Eltayeb M, Stride E, Edirisinghe M. Electrosprayed core-shell polymer-lipid nanoparticles for active component delivery. Nanotechnology 2013;24:465604.

[9] Yu DG, Wang X, Li XY, Chian W, Li Y, Liao YZ. Electrospun biphasic drug release polyvinylpyrrolidone/ ethyl cellulose core/sheath nanofibers, Acta Biomater 2013;9:5665-5672.

[10] Labbaf S, Deb S, Camma G, Stride E, Edirisinghe M. Preparation of multi-component drug delivery nanoparticles using a triple-needle electrohydrodynamic device. J Colloid Interf Sci 2013;409:245-254.

[11] Hubbell JA, Chikoti A. Nanomaterials for drug delivery. Science 2012;337:303-305.

[12] Perez RA, Kim HW. Core-shell designed scaffolds for drug delivery and tissue engineering. Acta Biomater 2015; 21: 2-19.

[13] Yu DG, Yang JH, Wang X, Tian F. Liposomes self-assembled from electrosprayinged composite microparticles. Nanotechnology 2012; 23:105606.

[14] Liu ZP, Cui L, Yu DG, Zhao ZX, Chen L. Electrosprayed core-shell solid dispersions of acyclovir fabricated using an epoxy-coated concentric spray head. Int J Nanomed 2014;9:1967-1977.

[15] Yu DG, Williams GR, Yang JH, Wang X, Yang JM, Li XY. Solid lipid nanoparticles self-assembled from electrosprayed polymer-based micoparticles. J Mater Chem 2011;21:15957-15961.

[16] Sun J, Xianyu Y, Jiang X. Point-of-care biochemical assays using gold nanoparticle-implemented microfluidics. Chem Soc Rev 2014;43:6239-6253.

[17] Hadinoto K, Sundaresan A, Cheow WS. Lipid-polymer hybrid nanoparticles as a new generation therapeutic delivery platform: a review. Eur J Pharm Biopharm 2013;85:427-443.

[18] Zhang L, Chan JM, Gu FX, Rhee JW, Wang AZ, Radovic-Moreno AF, Alexis F, Langer R, Farokhzad OC. Self-assembled lipid--polymer hybrid nanoparticles: a robust drug delivery platform. ACS Nano 2008; 2:1696-1702.

[19] Qin CC, Duan XP, Wang L, Zhang LH, Yu M, Dong RH, Yan X, He HW, Long YZ. Melt electrospinning of poly(lactic acid) and polycaprolactone microfibers by using a hand-operated wimshurst generator. Nanoscale 2015;7:16611-16615.

[20] Jiang H, Wang L, Zhu K. Coaxial electrospinning for encapsulation and controlled release of fragile water-soluble bioactive agents. J Control Release 2014;193: 296-303.

[21] Erickson AE, Edmondson D, Chang FC, Wood D, Gong A, Levengood SL, Zhang M. High-throughput and high-yield fabrication of uniaxially-alignedchitosan-based nanofibers by centrifugal electrospinning. Carbohydr Polym 2015;134:467-474.

[22] Jiang K, Long YZ, Chen ZJ, Liu SL, Huang YY, Jiang X, Huang ZQ. Airflow-directed in situ electrospinning of a medical glue of cyanoacrylate for rapid hemostasis in liver resection. Nanoscale 2014;6:7792-7798.

[23] Sun B, Long YZ, Zhang HD, Li MM, Duvail JL, Jiang XY, Yin HL, Advances in three-dimensional nanofibrous macrostructures via electrospinning. Prog Polym Sci 2014;39:862-890.

[24] Lu W, Sun J, Jiang X. Recent advances in electrospinning technology and biomedical applications of electrospun fibers. J Mater Chem B 2014;2:2369-2380.

[25] Wang SW, Chen W, He S, Zhao QL, Li XH, Sun JS, Jiang XY. Mesosilica-coated ultrafine fibers for highly efficient laccase encapsulation. Nanoscale 2014;6: 6468-6472.

[26] Yu DG, White K, Chatterton NP, Li Y, Li L, Wang X. Structural lipid nanoparticles self-assembled from electrospun core-shell polymeric nanocomposites. RSC Adv 2015;5:9462-9466.

[27] Nagy ZK, Balogh A, Démuth B, Pataki H, Vigh T, Szabó B, Molnár K, Schmidt BT, Horák P, Marosi G, Verreck G, Assche IV, Brewste ME. High speed electrospinning for scaled-up production of amorphous solid dispersion of itraconazole. Int J Pharm 2015;480:137-142.

[28] Kim SE, Wang J, Jordan AM, Shanda L, Korley TJ, Baer E, Pokorski JK. Surface modification of melt extruded poly(ε-caprolactone) nanofibers: toward a new

scalable biomaterial scaffold. ACS Macro Letters 2014;3:585-589.

[29] Balogh A, Cselkó R, Démuth B, Verreck G, Mensch J, Marosi G, Nagy ZK. Alternating current electrospinning for preparation of fibrous drug delivery systems. Int J Pharm 2015;495:75-80.

[30] Qian W, Yu DG, Li Y, Liao YZ, Wang X, Wang L. Dual drug release electrospun core-shell nanofibers with tunable dose in the second phase. Int J Mol Sci 2014;15:774-786.

[31] Yu DG, Li XY, Wang X, Yang JH, Annie Bligh SW, Williams GR. Nanofibers fabricated using triaxial electrospinning as zero order drug delivery systems. ACS Appl Mater Interfaces 2015;7:18891-18897.

[32] Chen H, Wang N, Di J, Zhao Y, Song Y, Jiang L. Nanowire-in-microtube structured core/shell fibers via multifluidic coaxial electrospinning. Langmuir 2010; 26:11291-11296.

[33] Yarin AL. Coaxial electrospinning and emulsion electrospinning of core–shell fibers. Polym Adv Technol 2011;22:310-317.

[34] Yarin AL, Zussman E, Wendorff JH, Greiner A. Material encapsulation and transport in core–shell micro/nanofibers,polymer and carbon nanotubes and micro/nanochannels. J Mater Chem 2007;17:2585-2599.

[35] Lee MW, An S, Lee C, Liou M, Yarin AL, Yoon SS. Hybrid self-healing matrix using core-shell nanofibers and capsuleless microdroplets. ACS Appl Mater Interfaces 2014;6:10461-10468.

[36] Wang X, Zhang WJ, Yu DG, Li XY, Yang H. Epoxy resin nanofibers prepared using electrospun core/sheath nanofibers as templates. Macromol Mater Eng 2013;298:664-669.

[37] Yu DG, Zhu LM, Branford-White C, Bligh SWA, White K. Coaxial electrospinning with organic solvent for controlling the self-assembled nanoparticle size. Chem Commun 2011;47:1216-1218.

[38] Agarwal S, Greiner A, Wendorff JH. Functional materials by electrospinning of polymers. Prog Polym Sci 2013;38:963-991.

[39] Zhang Z, Liu S, Xiong H, Jing X, Xie Z, Chen X, Huang Y. Electrospun PLA/MWCNTs composite nanofibers for combined chemo- and photothermal therapy. Acta Biomater 2015; 26:115-123.

[40] Yu DG,Williams GR, Wang X, Liu XK, Li HL, Bligh SWA. Dual drug release nanocomposites prepared using a combination of electrospraying and electrospinning. RSC Adv 2013;3:4652-4658.

[41] Su Y, Su Q, Liu W, Lim M, Venugopal JR, Mo X, Ramakrishna S, Al-Deyab SS, El-Newehy M. Controlled release of bone morphogenetic protein 2 and dexamethasone loaded in core-shell PLLACL-collagen fibers for use in bone tissue

engineering. Acta Biomater 2012;8:763-771.

[42] Yu DG, Branford-White C, Bligh SWA, White K, Chatterton NP, Zhu LM Improving polymer nanofiber quality using a modified co-axial electrospinning process. Macromol Rapid Commun 2011;32:744-750.

[43] Yu DG, Chian W, Wang X, Li XY, Li Y, Liao YZ. Linear drug release membrane prepared by a modified coaxial electrospinning process. J Membrane Sci 2013, 428, 150-156.

[44] Jiang S, Duan G, Zussman E, Greiner A, Agarwal S. Highly flexible and tough concentric tri-axial polystyrene fibers. ACS Appl Mater Interfaces 2014;6:5918-5923.

[45] Liu W, Ni C, Chase DB, Rabolt JF. Preparation of multilayer biodegradable nanofibers by tri-axial electrospinning. ACS Macro Lett 2013;2:466-468.

[46] Labbaf S, Ghanbar H, Stride E, Edirisinghe M. Preparation of multilayered polymeric structures using a novel four-needle coaxial electrohydrodynamic device. Macromol Rapid Commun 2014;35:618-623.

[47] Starr JD, Andrew JSA. Route to synthesize multifunctional tri-phase nanofibers. J Mater Chem C 2013;1:2529-2533.

[48] Zhao Y, Cao X, Jiang L. Bio-mimic multichannel microtubes by a facile method. J Am Chem Soc 2007;129:764-765.

[49] Han D, Steckl A. Triaxial electrospun nanofiber membranes for controlled dual release of functional molecules. ACS Appl Mater Interfaces 2013;5:8241-8245.

[50] Illangakoon UE, Yu DG, Ahmad BS, Chatterton NP, Williams GR. 5-fluorouracil loaded Eudragit fibers prepared by electrospinning. Int J Pharm 2015;495:895-905.

[51] Small DM. Phase equilibria and structure of dry and hydrated egg lecithin. J Lipid Res 1967;8:551-557.

[52] O'brien WM. Adverse reactions to nonsteroidal anti-inflammatory drugs. Diclofenac compared with other nonsteroidal anti-inflammatory drugs. Am J Med 1986;80(4B): 70-80.

[53] Gibofsky A. Low-dose SoluMatrix diclofenac: a review of safety across two phase III studies in patients with acute and osteoarthritis pain. Expert Opin Drug Saf 2015;25:1-13.

[54] Kawabata Y, Wada K,Nakatani M, Yamada S, Onoue S. Formulation design for poorly water-soluble drugs based on biopharmaceutics classification system: basic approaches and practical applications. Int J Pharm 2011;420:1-10.

[55] Ritschel WA, Koch HP, Alcorn GJ. In vivo-in vitro correlations with sustained-release theophylline preparations. Methods Find Exp Clin Pharmacol 1984;6:609-618.

[56] Kriwet K, Müller-Goymann CC, Diclofenac release from phospholipid drug systems and permeation through excised human stratum corneum. Int J Pharm 1995; 125:231-242

[57] Hamori M, Yoshimatsu S, Hukuchi Y, Shimizu Y, Fukushima K, Sugioka N, Nishimura A, Shibata N. Preparation and pharmaceutical evaluation of nano-fiber matrix supported drug delivery system using the solvent-based electrospinning method. Int J Pharm 2014; 464:243-251.

[58] Verreck G, Chun I, Peeters J, Rosenblatt J, Brewster ME. Preparation and characterization of nanofibers containing amorphous drug dispersions generated by electrostatic spinning. Pharm Res 2003; 20:810-817.

[59] Démuth B, Nagy ZK, Balogh A, Vigh T, Marosi G, Verreck G, Assche IV, Brewster ME. Downstream processing of polymer-based amorphous solid dispersions to generate tablet formulations. Int J Pharm 2015;486:268-286.

[60] Dzenis Y. Spinning continuous fibers for nanotechnology. Science 2004;304:1917-1919.

[61] Chen CH, Chen SH, Shalumon KT, Chen JP. Dual functional core-sheath electrospun hyaluronic acid/polycaprolactone nanofibrous membranes embedded with silver nanoparticles for prevention of peritendinous adhesion. Acta Biomater 2015; 26:225-235.

Table and Figures Legend

Table 1. Key details of the electrospinning processes and resultant fibers

Fig. 1. A diagram of the modified tri-axial electrospinning process and its use for preparing core-shell drug-loaded nanofibers.

Fig. 2. The implementation of modified tri-axial electrospinning: (a) the connection of the spinneret with the power supply and the working fluids (left), and images of the spinneret (insets); (b) a digital photograph of the tri-axial process (left), the droplet before a voltage of 15 kV was applied (top-right) and the compound Taylor cone (bottom-right).

Fig. 3. FESEM images of the core-shell nanofibers and their size distributions; (a1 and a2) F1; (b1 and b2) F2; (c1 and c2) F3; (d1 and d2) F4. The inset to (d1) shows a clump of PL-DS.

Fig. 4. (a) A FESEM image of the cross-sections of F2 and (b) a TEM image showing the same.

Fig. 5. XRD patterns of the raw materials (PL, EL100 and DS) and F2.

Fig. 6. ATR-FTIR spectra and the molecular formula of the fiber components.

Fig. 7. *In vitro* dissolution of DS and D2 (a) and the proposed drug release mechanism (b).

Fig. 8. (a) The transmittance of the dissolution medium measured at 500 nm as a function of time and (b) the sizes of the PL-DS particles measured by SDLC at the end of the dissolution experiment.

Fig. 9. *Ex vivo* permeation profiles of the F2 fibers and pure DS (n=6). It should be noted that it is not possible in the permeation experiment to distinguish between drug in solution and in very small particles (< 220 nm) which could pass through the filtration membrane used. Thus, some portion of the DS which had permeated in the "free in water" experiment could in fact be in very small nanoparticles.

Fig. 10. The feasibility of different tri-axial electrospinning processes.